The key role of heavy precipitation events in climate model disagreements of future annual precipitation changes in California

David W. Pierce[1,*]

Daniel R. Cayan[1]

Tapash Das[1,6]

Edwin P. Maurer[2]

Norman L. Miller[3]

Yan Bao[3]

M. Kanamitsu[1,+]

Kei Yoshimura[1]

Mark A. Snyder[4]

Lisa C. Sloan[4]

Guido Franco[5]

Mary Tyree[1]

19 February 2013 / Version 2

[1]*Scripps Institution of Oceanography, La Jolla, CA*

[2]*Santa Clara University, Santa Clara, CA*

[3]*University of California, Berkeley, Berkeley, CA*

[4]*University of California, Santa Cruz, Santa Cruz, CA*

[5]*California Energy Commission, Sacramento, CA*

[6]*CH2M HILL, Inc., San Diego, CA*

[+]Deceased

[*]Corresponding Author address: SIO/CASPO, Mail stop 0224, La Jolla, CA, 92093-0224. dpierce@ucsd.edu, 858-534-8276. Fax: 858-534-8561

ABSTRACT

Climate model simulations disagree on whether future precipitation will increase or decrease over California, which has impeded efforts to anticipate and adapt to human-induced climate change. This disagreement is explored in terms of daily precipitation frequency and intensity. It is found that divergent model projections of changes in the incidence of rare heavy (> 60 mm/day) daily precipitation events explain much of the model disagreement on annual timescales, yet represent only 0.3% of precipitating days and 9% of annual precipitation volume. Of the 25 downscaled model projections we examine, 21 agree that precipitation frequency will decrease by the 2060s, with a mean reduction of 6-14 days/year. This reduces California's mean annual precipitation by about 5.7%. Partly offsetting this, 16 of the 25 projections agree that daily precipitation intensity will increase, which accounts for a model average 5.3% increase in annual precipitation. Between these conflicting tendencies, 12 projections show drier annual conditions by the 2060s and 13 show wetter. These results are obtained from sixteen global general circulation models downscaled with different combinations of dynamical methods (WRF, RSM, and RegCM3) and statistical methods (BCSD and BCCA), although not all downscaling methods were applied to each global model. Model disagreements in the projected change in occurrence of the heaviest precipitation days (> 60 mm/day) account for the majority of disagreement in the projected change in annual precipitation, and occur preferentially over the Sierra Nevada and Northern California. When such events are excluded, nearly twice as many projections show drier future conditions.

1. Introduction

California has taken an aggressive approach to confronting human-induced climate change (e.g., Anderson et al. 2008, Franco et al. 2011). For example, state assembly bill 32 (AB 32) targets reducing greenhouse gas emissions to 1990 levels by 2020. Actions are also being taken to adapt to the anticipated changes, such as taking sea level rise into account in coastal planning.

While it is nearly certain that California's climate will warm in future decades (e.g., Hayhoe et al. 2004; Leung et al. 2004; IPCC, 2007; Pierce et al. 2012), projections of annual precipitation change are proving more problematic. Model results diverge significantly, with a model-mean value near zero (e.g., Dettinger 2005). Although a projection of no significant change is as valid as any other, it is worth exploring the origins of this disagreement. We approach the problem using a variety of global models and downscaling techniques to examine how changes in precipitation frequency and intensity on a daily timescale combine to produce the annual change.

Changes in the frequency and intensity of precipitation events can have a profound impact. Precipitation frequency can affect crops, tourism, and outdoor recreation. More intense rainfall increases the chance of flooding and, lacking adequate reservoir storage, can mean that a larger proportion of total precipitation leaves the region through runoff, becoming unavailable for beneficial use. More intense rainfall and the transition from snow to rain may also reduce groundwater recharge in some locations (Dettinger and Earman, 2007).

Numerous studies have examined projected changes in California's monthly or seasonal precipitation due to human-induced climate change, but only a few have examined daily precipitation intensity and frequency (Kim 2005; Hayhoe et al. 2004; Leung et al. 2004). However, the physical processes causing changes in the frequency and intensity of daily precipitation have become better understood in recent years. Warmer air temperatures allow more water vapor in the atmosphere, providing a tendency towards more intense precipitation, although the actual processes controlling extremes depend on changes in temperature, upward velocity, and precipitation efficiency (O'Gorman and Schneider 2009; Muller et al. 2011). Evidence from energy and water balance constraints (Stephens and Hu 2010) and global climate models (Meehl et al. 2005) indicates that climate warming will generally result in greater intensity precipitation events, though it is less clear how these changes will play out regionally. For example, in the region of interest here, the migration of storm tracks poleward implies a shift in precipitation frequency over the west coast of the U.S. (e.g., Yin 2005; Salathe 2006; Ulbrich et al. 2008; Bender et al. 2012).

In California some of the projected precipitation changes, particularly in daily extremes, are related to atmospheric rivers of water vapor that originate in the tropics or subtropics and are advected by winds into the west coast of North America (e.g., Ralph and Dettinger 2011). Changes in atmospheric rivers (Dettinger 2011) would be important because they generate many of California's large floods, and play an key role in delivering the state's water supply (Ralph and Dettinger 2011, 2012).

Global models can reproduce some large scale patterns of precipitation and its variability, but typically simulate light precipitation days too frequently and heavy precipitation days too weakly (Sun et al. 2006, Dai et al. 2006). This problem is resolution-dependent; Wehner et al. (2010) showed that intensity is captured better as model resolution increases from 2 to ~0.5 degree. Chen and Knutson (2008) emphasized the fundamental problems of comparing station precipitation observations, which are valid at a point, to climate model fields, which are averaged over a gridcell.

Downscaling is often used to address the problem of global model resolution that is too coarse to simulate precipitation intensity accurately. Downscaling is especially needed given California's coastal and interior mountain ranges, which affect precipitation yet are poorly resolved by global climate models. Downscaling can use either statistical methods, which are based on observed relationships between small-scale and large-scale processes, or dynamical methods, which use regional fine-scale climate or weather models driven by global climate models.

Our first goal is to show how downscaled climate simulations project future changes in daily precipitation frequency and intensity over California, and how these combine to produce annual precipitation changes. Since our interest is in water supply issues, we focus on absolute changes using a single threshold for heavy precipitation events across the state, rather than on percentage changes in precipitation relative to the local climatology. (Other investigators might be more interested in the largest local fractional changes, for instance how they affect the local ecology.) This means that our analysis also ends up focusing on locations

where heavy precipitation occurs, which in California is the Sierra Nevada and northern part of the state. An analysis that finds heavy precipitation events are important is necessarily intertwined with the location where such events can happen, which is a function of how the regional meteorological setting (prevalent moisture-bearing wind patterns, for example) interacts with the local topography.

The second goal is to compare how different statistical and dynamical downscaling methods produce changes in precipitation frequency and intensity. We use daily precipitation from two global models dynamically downscaled with three regional climate models, those two same global climate models along with two others statistically downscaled by a technique that preserves the daily sequence of global model precipitation, and those 4 global models along with 12 more statistically downscaled with a technique that is widely used but does not preserve the daily sequence of precipitation.

Due to the computational burden of dynamically downscaling with multiple regional models, we limit our analysis to two periods: the historical era (1985-1994) and the 2060s. For the same reason we consider only the SRES A2 emissions forcing scenario (Nakicenovic et al. 2000). The 2060s is about the last decade where the change in global air temperatures due to anthropogenic forcing is not well separated between different emissions scenarios (IPCC 2007). The same models were used in Pierce et al. (2012) to examine projected seasonal mean and 3-day maximum temperature and precipitation changes in California; this work extends that previous study by examining how changes in precipitation frequency and intensity on a daily timescale combine to produce overall precipitation changes.

2. Data and Methods

The models and downscaling methods used in this work are the same as used in Pierce et al. (2012); we refer the reader to that work for a detailed description. All downscaling is to a ~12 km spatial resolution. In cases where more than one ensemble member was available for downscaling, we used ensemble number 1 from the global model.

The global models and downscaling methods applied to each are listed in Table 1. Each combination of global model and downscaling technique will be referred to as a "model projection". Dynamically downscaled results are obtained using three regional climate models (RCMs): 1) Version 3 of the Regional Climate Model (RegCM3), which is originally based upon the MM5 mesoscale model (Pal et al. 2007). 2) The NCAR/NCEP/FSL Weather Research and Forecasting (WRF) model (Skamarock et al. 2008). 3) The Regional Spectral Model (RSM, Kanamitsu et al. 2005), which is a version of the National Centers for Environmental Prediction (NCEP) global spectral model optimized for regional applications. The ability of the regional models to reproduce observed climatology given historical reanalysis as forcing was examined in Miller et al. (2009), who concluded that while all the models have limitations, they do a credible job overall. In total, we examine five dynamically downscaled model projections.

Two methods of statistical downscaling are used: 1) Bias Correction with Constructed Analogues (BCCA; Hidalgo et al. 2008; Maurer et al. 2010), which downscales fields by linearly combining the closest analogues in the historical record. 2) Bias Correction with Spatial Disaggregation (BCSD; Wood et al. 2002, 2004), which generates daily data from monthly GCM output by selecting a

historical month and rescaling the daily precipitation to match the monthly value, and so does not preserve the original global model sequence of daily precipitation. The historical month chosen is conditioned on monthly precipitation amount, so the number of zero precipitation days can change as precipitation changes, but the precipitation intensity changes in BCSD are less directly connected to the GCM results than in the other methods. Maurer and Hidalgo (2008) compared results of using BCCA and BCSD, and concluded that they have comparable skill in producing downscaled monthly temperature and precipitation. In total, we analyze 4 model projections with BCCA, and another 16 with BCSD.

BCCA and BCSD downscale to the same 1/8° x 1/8° (~12 km) latitude-longitude grid used in the Hamlet and Lettenmaier (2005) observational data set. RegCM3, WRF, and RSM each have their own fine-scale grid of *O*(12 km) but are not coincident. For consistency and ease of comparison with observations, the dynamically downscaled fields were regridded to the same 1/8° x 1/8° latitude-longitude grid used by the statistical methods and observations before analysis.

Natural climate variability due to such phenomena as the El Nino/Southern Oscillation (ENSO) and the Pacific Decadal Oscillation (PDO) is not of direct interest here, so in order to minimize these effects we generally average our results over multiple model projections. Since different projections have different phases of ENSO, PDO, or other natural climate modes of variability, averaging across model projections tends to reduce the influence of natural variability on our results.

2.1 Bias correction

Biases in downscaled precipitation fields can lead to inaccurate hydrological impacts, especially given the non-linear nature of runoff. Since the project's purpose was to focus on hydrological and other applications, all the precipitation fields shown here are bias corrected (Panofsky and Brier 1968; Wood et al. 2002, 2004; Maurer 2007; Maurer et al. 2010). Such biases can be created by the downscaling method, but often reflect biases in the original global model (e.g., Wood et al. 2004, Duffy et al. 2006, Liang et al. 2008). Details of the bias correction procedure are given in Pierce et al. (2012).

3. Results

3.1 Change in precipitation frequency

Current GCMs over-predict the number of days with a small amount of precipitation (e.g., Sun et al. 2006, Dai 2006; Chen and Knutson, 2008; cf. Wehner et al. 2010). Typically this problem is addressed by defining a threshold below which a model is considered to have zero precipitation. For example, Leung et al. (2004) used 0.01 mm/day, Caldwell et al. (2009) used 0.1 mm/day, and Kim (2005) used 0.5 mm/day. Station observations have limited resolution too; in the global summary of day (GSOD) data set no values less than 0.25 mm/day are reported, while NOAA's co-operative observing stations typically report no values less than 0.1 mm/day. We use a threshold of 0.1 mm/day below which model precipitation values are taken to be zero.

Figure 1 shows the climatological frequency (days/year) of days with precipitation less than 0.1 mm/day, hereafter referred to as “zero precipitation days”. Panel a) is the mean across all model simulations for the historical period, and panel b) is from the Hamlet and Lettenmaier (2005) observations over the period 1970-99. The two fields are similar, but all model fields are bias corrected (Pierce et al. 2012), which reduces the disagreement between models and observations. It makes little sense to reformulate a non-bias corrected version of BCSD or BCCA, but the dynamical downscaling methods apply bias correction after the simulations are performed. Panels c) and d) of Figure 1 show the number of zero precipitation days from the dynamically downscaled models with and without bias correction, respectively. With bias correction the number of zero-precipitation days matches observations much better than before bias correction, even though the precipitation rate is bias corrected rather than the number of zero precipitation days. The non-bias corrected fields have too few zero precipitation days. Besides the propensity for models to simulate too many light precipitation days, this reflects the tendency of dynamic downscaling in this region to produce more precipitation than observed (Miller et al., 2009). Panel e) shows histograms of percentage of gridpoints in the domain that experience the indicated rate of zero-precipitation days/year. The non-bias corrected histogram (green triangles) is a poor representation of the observed distribution (red circles). Bias correction improves this substantially (purple crosses), although differences in the distributions are still evident, particularly around 220 and 270 days/year.

Figure 2 shows the change (future minus historical) in annual precipitation amount and frequency of zero-precipitation days along with the empirical cumulative distribution function (CDF) of these quantities. All values are

averaged across model projections. The number of zero-precipitation days increases by 6-14 days per year over most of the domain, especially Northern California and the Sierra Nevada, which is an increase of 3-6% (Figure 2e). Yet model-mean precipitation in this region increases slightly, which implies that precipitation intensity has increased. Similarly, the southern coastal regions show pronounced drying, but do not show the largest increase in zero-precipitation days. Overall, 73% of the gridcells experience decreasing precipitation, and the median change in number of zero-precipitation days is 8 days/year (about a 3% increase).

The effect of each downscaling technique on the change in number of zero precipitation days is shown in Figure 3, illustrated for the two global models that were downscaled with the most techniques (CCSM3 and GFDL CM2.1). The original global model field is shown in the leftmost column for comparison. BCSD tends to show the least increase in zero-precipitation days while BCCA tends to show the most, although the differences are small. The decreasing number of zero-precipitation days in the interior southeast with RSM downscaling is associated with a more active North American monsoon. As discussed in Pierce et al. (2012), this is primarily a summer response that is seen more clearly with dynamical downscaling than statistical downscaling, and is relatively more influenced by the individual dynamic downscaling model being used then by the global GCM being downscaled. This suggests that the details of the projected summer monsoonal changes are sensitive to the cloud and precipitation parameterizations used in the regional dynamical models.

3.2 Effect of downscaling on daily precipitation intensity

Figure 4 shows the way different downscaling techniques alter the global model's daily precipitation intensity. The colored maps show the ratio of downscaled precipitation rate in a gridcell to the global model's precipitation rate on the same day and interpolated to the same gridcell, averaged over days with precipitation. We term this the "amplification factor." The line plots show histograms of the amplification factor across all gridcells for each downscaling technique. BCSD results are excluded since they do not preserve the daily sequence of GCM precipitation. Results are broken out by low, medium, and high tercile of the original global model precipitation intensity in the gridcell.

The amplification factor varies spatially and non-linearly with the magnitude of the GCM's precipitation. Each dynamical downscaling method changes the global model precipitation signal in a characteristic way, though all amplify the global model's precipitation rate in the lowest tercile. In the Sierra Nevada and the northern coastal mountains, dynamic downscaling amplifies precipitation rates in the low tercile by 4 or more compared to the original GCM. In the medium and high terciles the dynamically downscaled simulations exhibit successively greater fractional precipitation rate reductions in rain shadow regions with respect to the original GCMs. In such locations the GCMs typically produce unrealistically heavy precipitation due to adequately resolved topography.

The amplification factors of the three dynamical methods are similar to each other, and all differ from the BCCA statistical method, a feature particularly evident in the histograms. BCCA has a more linear relationship between global and downscaled precipitation intensity, especially in mountainous terrain such as

the Sierra Nevada and coastal range, where non-linearities in the dynamical methods are pronounced.

The largest non-linearities in BCCA's amplification factor are in the rain shadow regions. The real world shows this behavior as well; an analysis of the Hamlet and Lettenmaier (2005) data shows that as regional averaged precipitation increases, the contrast between precipitation in the mountains and precipitation in the rain shadow increases as well (not shown). BCCA, being based on observations, mimics this behavior.

3.3 Future change in daily precipitation intensity

Figure 5 shows the change (future minus historical) in the fraction of precipitating days that have precipitation of the indicated intensity (mm/day), averaged across all model projections. In most locations the fractional occurrence of amounts less than 10 mm/day decreases. However this is compensated for by a greater occurrence of days with 20 mm/day or more. Over much of the dry interior, values greater than 100% indicate that when considering only days with precipitation, the rate of days with heavy precipitation more than doubles. Elsewhere, such days typically increase by 25-50%.

Figure 2 showed that the number of days with precipitation generally declines, so the increase in fraction of precipitating days with heavy precipitation does not necessarily mean that the actual number of days per year with heavy precipitation increases. (I.e., if it rains half as often, but the fraction of rainy days that have heavy rain doubles, then the number of heavy rain days per year is unchanged.) To clarify this, Figure 6 shows the change in precipitation intensity expressed as the

change (future minus historical) in number of days per year, averaged across model projections. Over most of California, especially the Sierra Nevada and North Coast regions (which experience most of California's precipitation) the number of days with 0.1 to 20 mm/day of precipitation decreases, while days with 60 mm/day or more increase. Because heavy precipitation days are rare the increase in number of days per year is low. In all classes of precipitation intensity, Southern California experiences the least changes (Figure 6, right panel), while Nevada experiences the greatest decrease in light precipitation days and Northern California experiences the greatest increase in heavy precipitation days.

The effect of downscaling technique on changes in precipitation intensity is shown in Figure 7. For brevity, only changes in the lowest (0.1-5 mm/day) and highest (60+ mm/day) intensity bins from Figure 6 are shown. The downscaled change in California's average annual precipitation computed by each method is given in the panel title, for reference. Away from the summer monsoon region, the different downscaling techniques consistently simulate fewer light precipitation days in both global models. However results for the strongest precipitation intensities are not consistent, either across different downscaling techniques or for different global models across a single downscaling technique. This suggests that inconsistencies in the way changes in heavy precipitation events are simulated could be an important source of model disagreement on future precipitation changes, a point explored further below. For GFDL, the different downscaling methods produce annual mean changes of −16.6 to −2.3%; for CCSM3, the range is −17.9 to 8.7%. Therefore, we see that even given the same global model data as input, downscaling can produce a wide range of net annual precipitation changes.

3.4 The combined effect of frequency and intensity

The projected change in California's annual mean precipitation shows little agreement across models (e.g., Dettinger 2005). Yet our results indicate that models agree that precipitation frequency will decrease and (to a lesser extent) daily intensity will increase. Since the annual precipitation amount is determined by the frequency and intensity of precipitation events, is this a contradiction?

To sensibly compare the effects of changes in frequency and intensity on annual precipitation requires expressing quantities in the same units. We linearize the problem by assuming that that loss of a precipitating day in the future decreases the total annual precipitation by an amount equal to the average rainy-day precipitation in that day's month during the historical period. (The day's month is used because, for example, loss of a July precipitating day typically has less effect on the annual average than loss of a February precipitating day.) The effects of changes in precipitation intensity are then calculated as the actual change in precipitation minus the contribution due to the change in number of precipitating days.

Figure 8 shows the effect of the change in California-averaged precipitation frequency (panel a) and intensity (panel b) on total annual precipitation (panel c). Of the 25 model projections, 21 show a negative tendency in annual precipitation due to fewer days with precipitation, with a mean decline of 32 mm/year (5.7% of the annual total precipitation of 557 mm). Sixteen model projections show greater precipitation intensity, which accounts for an increase of 29 mm/year (5.3%) in the annual total. When these competing tendencies are added together the results are distributed around zero, with 12 models showing drier future conditions and

353 13 showing wetter. Although the small sample of BCCA results prevents
354 definitive conclusions, Figure 8b suggests that BCCA may produce less increase
355 in precipitation intensity than other methods. (This is consistent with Figure 7 for
356 the CCSM3 model, but not for GFDL.)

357 The inference from Figure 7 was that model disagreement between projected
358 changes in California's annual precipitation may arise from the relatively few
359 precipitation events > 60 mm/day. This can be tested by computing the change in
360 annual precipitation only including gridcells and days ("gridcell-days") when the
361 gridcell's daily precipitation is less than some cutoff value. Results are shown in
362 Figure 9, with the precipitation cutoff increasing from 5 to 60 mm/day. At the
363 lower cutoffs, the models overwhelmingly agree on the sign of the annual change.
364 Even when all gridcell-days with precipitation less than 60 mm/day are included
365 (99.7% of all possible gridcell-days), almost 1.8 times as many models show a
366 precipitation decrease as an increase. Only when the final 0.3% of gridcell-days
367 with heaviest precipitation are included do the models disagree, with half showing
368 an annual precipitation increase and half showing a decrease. These events occur
369 only rarely, but have a strong influence on the annual precipitation change.

370 Precipitation events > 60 mm/day occur preferentially in the Sierra Nevada and
371 Northern Coastal regions (Figure 10; cf. Ralph and Dettinger 2012). On average,
372 they occur about 1 in every 50-200 days in the Northern Coastal and Sierra
373 Nevada regions. When considering precipitating days only (Figure 10b), such
374 events are about 1 in every 10-50 precipitating days in the North Coast, Sierra
375 Nevada, and Los Angeles coastal mountain regions. The Hamlet and Lettenmaier
376 (2005) data set indicates that typically about 9% of California's total annual

precipitation volume falls during such days. The cumulative distribution functions (Figure 10c) indicate that as the relationship between the occurrence rate (expressed as a 1-in-N days rate) and the fraction of gridcells experiencing that occurrence rate or higher is approximately exponential. In other words, high occurrence rates (small N) are concentrated in a small region, and the occurrence rate drops dramatically as more grid cells are considered.

3.5 Changes in precipitation frequency and intensity over the year

Most of California's precipitation falls during the cool months (October through April). Figure 11 shows the change in precipitation by month (top row), change in the number of days with non-zero precipitation (middle row), and 50th and 95th percentiles of precipitation on days with non-zero precipitation (bottom row). Values are averaged over four representative climate regions identified by Abatzoglou et al. (2009; Figure 12), which are based on the covariance of anomalous precipitation and temperature over the state. Only BCCA and dynamically downscaled data have been used in this analysis, since those preserve the daily sequence of precipitation from the original global models. (In a sensitivity test we recomputed this figure using BCSD data, and found little difference except in summer in the North American monsoon region, where BCSD does not show the pronounced tendency towards wetter conditions.) Figure 2 showed that zero precipitation days increase over most of the domain, but Figure 11 shows this does not happen uniformly over the year. Virtually the entire state has a statistically significant drop in spring precipitation (Figure 11, top row), particularly in April. This is accompanied by a decrease in precipitating days (Figure 11, middle row), although this decrease is not always statistically

significant. This pattern is repeated, although more weakly, in the autumn: most regions show decreasing precipitation associated with fewer precipitating days.

Most of the regions, with the exception of the Anza-Borrego, show a tendency towards increasing 95th percentile precipitation during some or all of the cool season months (Nov-Mar; bottom row of Figure 11). Winter average precipitation increases despite fewer precipitating days because precipitation events intensify.

Although this result is obtained with data pooled across the BCCA and dynamical downscaling techniques, the models do not all agree on this result. Of the four global models (CCSM3, GFDL 2.1, PCM1, and CNRM CM3), CCSM3 shows the strongest increase in winter precipitation intensity. GFDL 2.1 and PCM1 show weaker increases in intensity along the coast and decreases in the far Northeast, while CNRM shows mild decreases in storm intensity (and winter decreases in precipitation of 8-45%, mostly due to fewer days with precipitation) throughout the state.

The Anza-Borrego (Figure 11) and Inland Empire regions (not shown), which are affected by the North American monsoon, experience an increase in summer (JJA) precipitation that is associated with an increase in both precipitation frequency and intensity. Because of the spread of responses across the models, these changes are not statistically significant. CCSM3 and GFDL show these increases strongly, while CNRM shows only a weak increase and PCM shows a slight decrease.

3.6 Summary of changes in California precipitation frequency and intensity

The overall effect of seasonal changes in daily precipitation intensity and frequency is shown in Figure 13. Equivalent changes in seasonal precipitation (cm) are calculated as in section 3.4 (so that all values have the same units), and results averaged across all model projections. Each region's change in future precipitation is equal to the sum of changes due to the number of precipitating days and changes due to precipitation intensity.

In winter and spring almost all locations show an increase in daily precipitation intensity, except for the southern part of the state in winter. At the same time, almost all locations and seasons show a decrease in the number of precipitating days, except for summer, where there are few precipitating days in California to begin with. The exception is the southeastern part of the state in summer, which shows more precipitating days. The way the opposing tendencies of precipitation frequency and intensity combine yields a complex pattern of seasonal precipitation changes. In the northern part of the state in winter, the increase in storm intensity is stronger than the decrease in number of precipitating days, resulting in an overall mild (3-6%) increase in seasonal precipitation. In spring (MAM) a mild increase in daily precipitation intensity coupled with a strong decrease in number of precipitating days yields a significant tendency towards less precipitation (declines of > 10%). This can also be seen in autumn (SON), although the changes in storm intensity are small in this season. Finally, the southeastern part of California, on the edge of the region affected by the North American monsoon, shows both a mild increase in storm intensity and strong

445 increase in number of precipitating days in summer (JJA), resulting in large (>
446 100%) increases in that season's precipitation.

447 4. Summary and Conclusions

448 This work has evaluated future changes in daily precipitation intensity and
449 frequency in California between the historical period 1985-1994 and the 2060s.
450 Our goal is to see how model disagreements in projected annual precipitation
451 changes are expressed at the daily timescale.

452 We used data from 16 global climate models (GCMs) downscaled with a
453 combination of statistical (BCCA and BCSD) and dynamical (WRF, RCM, and
454 RegCM3) techniques, although not all downscaling techniques were applied to
455 each global model. We analyzed 25 model projections in total, where a model
456 projection is a unique combination of global model and downscaling technique.
457 We used the SRES A2 greenhouse gas and anthropogenic aerosols emissions
458 scenario, and equally weighted all model projections, since there is currently no
459 basis in the published literature for weighting different downscaling techniques
460 differently.

461 Our interest here is in water supply issues, so we focus on changes in total
462 statewide precipitation rather than fractional changes relative to the local
463 climatology. Twelve models project less annual precipitation and 13 project more.
464 The root of these differences is the way each model combines changes in
465 precipitation frequency and daily precipitation intensity.

466 The model projections agree that substantial portions of California, particularly in
467 the Sierra Nevada and North Coastal regions (which receive the majority of the

state's precipitation) will have 6-14 fewer precipitating days/year. Over the northern half of the state, this represents a decline of about 8-15%. Twenty-one of the 25 projections agree on the sign of this decline.

Most of the model projections also agree that daily precipitation intensity will increase. Expressed as a fraction of the number of days that experience precipitation, the incidence of days with precipitation greater than 20 mm/day increases by 25-100% over almost the entire domain considered here. Expressed as an incidence rate over all days of the year (not just precipitating days), precipitation rates below 10 mm/day decrease over nearly all of California, while most models project an increase in events of 60 mm/day or more over the Sierra Nevada and Northern Coastal regions. This has implications for flood management (Das et al. 2011), particularly as winter precipitation transitions from rain to snow (e.g., Knowles 2006) and the snow melts earlier in the year (e.g., Kim 2005, Hayhoe 2004, Das et al. 2009). Heavier precipitation could also increase the fraction of precipitation that generates surface runoff, reducing groundwater recharge (Dettinger and Earman, 2007).

Where the models disagree is whether the increase in precipitation intensity is sufficient to overcome the drying effects of fewer precipitating days. This disagreement arises largely from differences in the change in occurrence of events with precipitation > 60 mm/day. The largest absolute (i.e., not fractional) changes in such heavy precipitation events occur preferentially in the Sierra Nevada and northern California. The importance of changes in the incidence of heavy precipitation events is thus tied to the importance of locations where such events are relatively common. When such events are excluded, 1.8 times as many model

projections show declining annual precipitation in California as increasing. When they are included, the model projections are about split between drier and wetter future conditions. The change in incidence of these heavy precipitation events depends on both the global model and downscaling technique.

Events of this magnitude are rare, constituting only about 9% of annual precipitation volume and 1 in every 10-50 precipitation events in the Sierra Nevada, Northern Coastal, and California coastal ranges, and are almost unknown elsewhere. This implies that efforts to narrow the range of future precipitation projections over California need to focus on the models' representation of the rarest, heaviest precipitation events, how such events might be enabled by the interaction of the regional meteorological setting with local topography, and the fidelity of the models' atmospheric rivers (Zhu and Newell 1998). Atmospheric rivers play a key role in heavy-precipitation over many parts of the world (e.g., Lavers et al. 2011; Neiman et al. 2011; Dettinger et al. 2011; Viale and Nuñez 2011; Krichak et al. 2012), so our results could apply to other regions as well.

Winter precipitation increases in the northern part of the state are driven by significant increases in daily precipitation intensity with only mild decreases in the number of precipitating days, while spring and autumn decreases in precipitation are driven by fewer precipitating days with only mild increases in precipitation intensity. The change in number of precipitating days may be related to the poleward movement of the storm tracks expected under human-induced climate change (e.g., Yin 2005; Salathe 2006; Ulbrich et al. 2008; Bender et al. 2012). In the southern part of the state, although many simulations exhibit moderate increases in winter precipitation intensity, these increases are offset and

516 in several cases overwhelmed by decreases in the number of precipitating days.
517 Overall, the water supply effects of the tendency of the snowpack to melt earlier
518 in spring will be exacerbated by a decrease in spring precipitation. A similar
519 finding for the headwaters of the Colorado River was obtained by Christensen and
520 Lettenmaier (2007).

521 The dynamical downscaling techniques (WRF, RSM, and RegCM3) produced a
522 non-linear amplification of the global precipitation rate, with smaller rates of
523 global precipitation amplified the most. If this leads the dynamical techniques to
524 keep the soil more saturated than when BCCA downscaling is used, it could affect
525 the runoff efficiency (fraction of precipitation that generates runoff) that is
526 simulated when using different downscaling techniques. This could be usefully
527 explored in future work.

528 Finally, we note that projected future changes in California's annual precipitation
529 are generally small compared to either natural interannual climate variability or
530 the spread between different model projections (e.g., Dettinger 2005, Pierce et al.
531 2012). These results show that divergent model estimates of future annual
532 precipitation may be composed of individual seasonal changes in daily
533 precipitation intensity and frequency that have a specific geographical setting and
534 are much more consistent across models. Future attempts to examine whether
535 human-induced climate change is measurably affecting California's precipitation
536 might find identifiable changes in these other aspects of the precipitation field
537 long before the net annual change becomes evident.

Acknowledgements

This work was funded by the public interest energy research (PIER) program of the California Energy Commission (CEC), grant 500-07-042 to the Scripps Institution of Oceanography at UC San Diego: Development of probabilistic climate projections for California. DWP also received partial support from the Department of Energy, award DE-SC0002000 to examine future changes in climate model precipitation events, and the International ad-hoc Detection and Attribution (IDAG) project in furtherance of work to examine how daily timescale precipitation events change to accomplish low frequency, global climate changes. Partial salary support for TD from the CALFED Bay-Delta Program funded-postdoctoral fellowship grant, and for DRC and MT from the NOAA through the California Nevada Applications Program RISA activity is also acknowledged. We thank the global modeling groups that contributed data to the CMIP-3 archive; without their efforts and generosity in sharing the data, this work would have been impossible. The manuscript was improved by the comments of two anonymous reviewers, whom we thank for their contributions.

References

Abatzoglou, J. T., K. T. Redmond, and L. M. Edwards, 2009: Classification of Regional Climate Variability in the State of California. *J. App. Meteor. Clim.*, **48**, 1527-1541.

Anderson, J., F. Chung, M. Anderson, L. Brekke, D. Easton, et al., 2008: Progress on incorporating climate change into management of California's water resources. *Clim. Change,* **87** (Suppl 1): S91–S108, DOI 110.1007/s10584-10007-19353-10581.

Bender, F. A. M., V. Ramanathan, and G. Tselioudis, 2012: Changes in extratropical storm track cloudiness 1983-2008: observational support for a poleward shift. *Clim. Dyn.*, **38**, 2037.

Caldwell, P., H. N. S. Chin, D. C. Bader, and G. Bala, 2009: Evaluation of a WRF dynamical downscaling simulation over California. *Clim. Change,* **95**, 499-521

Chen, C-T., and T. Knutson, 2008: On the verification and comparison of extreme rainfall indices from climate models. *J. Clim.*, **21**, 1605-21.

Christensen, N. S., and Lettenmaier, D. P., 2007: A multimodel ensemble approach to assessment of climate change impacts on the hydrology and waer resources of the Colorado River basin. *Hydrol., Earth Sys. Sci.,* **11**, 1417-34.

Dai, A., 2006: Precipitation characteristics in eighteen coupled climate models. *J. Clim.*, **19**, 4605-30.

574 Das, T., M. D. Dettinger, D. R. Cayan, and H. G. Hidalgo, 2011: Potential
575 increase in floods in Californian Sierra Nevada under future climate projections.
576 *Clim. Change,* **109** (Suppl 1), S71-94.

577 Dettinger, M. D., 2005: From climate-change spaghetti to climate-change
578 distributions for 21st century California. *San Fran. Estuary Watershed Sci*., **3**,
579 Issue 1, article 4. 14 pp.

580 Dettinger, M. D., and S. Earman S, 2007: Western ground water and climate
581 change—Pivotal to supply sustainability or vulnerable in its own right? *Ground*
582 *Water News and Views, Assoc. Ground Water Scientists Engineers*, **4**, 4-5.

583 Dettinger, M. D., 2011: Climate change, atmospheric rivers and floods in
584 California—A multimodel analysis of storm frequency and magnitude changes. *J.*
585 *Am. Water Resour. Assoc*., **47**, 514-23.

586 Dettinger, M. D., F. M. Ralph, T. Das, P. J. Neiman, and D. R. Cayan, 2011:
587 Atmospheric rivers, floods and the water resources of California. *Water*, **3**, 445–
588 478, doi:10.3390/w3020445.

589 Duffy, P. B., R. W. Arritt, J. Coquard, W. Gutowski, J. Han, et al., 2006:
590 Simulations of present and future climates in the western United States with four
591 nested regional climate models. *J. Clim.*, **19**, 873-895.

592 Franco, G., D. Cayan, S. C. Moser, M. H. Hanemann, and M. A. Jones, 2011:
593 Second California Assessment: Integrated Climate Change Impacts Assessment of
594 Natural and Managed Systems - An Introduction. *Clim. Change*, **109** (Suppl. 1),
595 DOI: 10.1007/s10584-011-0318-z.

596 Hamlet, A. F., and D. P. Lettenmaier, 2005: Production of temporally consistent
597 gridded precipitation and temperature fields for the continental United States. *J.*
598 *Hydromet*., **6**, 330-336.

599 Hayhoe, K., D. Cayan, C. B. Field, P. C. Frumhoff, et al., 2004: Emissions
600 pathways, climate change, and impacts on California. *Proc. Nat. Acad. Sci.*, **101**,
601 12422-27.

602 Hidalgo, H. G., M. D. Dettinger, and D. R. Cayan, 2008: Downscaling with
603 Constructed Analogues: Daily precipitation and temperature fields over the United
604 States. California Energy Commission technical report CEC-500-2007-123. 48 pp.

605 IPCC, 2007: Climate change 2007: The physical science basis. Working group I
606 contribution to the fourth assessment report of the Intergovernmental Panel on
607 Climate Change. Cambridge University Press, Cambridge, United Kingdom and
608 New York, USA. 996 pp.

609 Kanamitsu, M., H. Kanamaru, Y. Cui, H. Juang, 2005: Parallel implementation of
610 the regional spectral atmospheric model. California Energy Commission technical
611 report CEC-500-2005-014. http://www.energy.ca.gov/2005publications/CEC-500-
612 2005-014/CEC-500-2005-014.

613 Kim, J., 2005: A projection of the effects of the climate change induced by
614 increased CO2 on extreme hydrologic events in the western U.S. *Clim. Change*,
615 **68**, 153-168.

616 Krichak, S. O., J. S. Breitgand, and S. B. Feldstein, 2012: A Conceptual Model for
617 the Identification of Active Red Sea Trough Synoptic Events over the

618 Southeastern Mediterranean. *J. Appl. Meteor. Climatol*., **51**, 962–971, doi:
619 http://dx.doi.org/10.1175/JAMC-D-11-0223.1.

620 Lavers, D. A., R. P. Allan, E. F. Wood, G. Villarini, D. J. Brayshaw, and A. J.
621 Wade, 2011: Winter floods in Britain are connected to atmospheric rivers.
622 *Geophys. Res. Lett.*, **38**, L23803, doi:10.1029/2011GL049783.

623 Leung, L. R., Y. Qian, X. D. Bian, W. M. Washington, J. G. Han, and J. O. Roads,
624 2004: Mid-century ensemble regional climate change scenarios for the western
625 United States. *Clim. Change*, **62**, 75-113.

626 Liang, X. Z., K. E. Kunkel, G. A. Meehl, R. G. Jones, and J. X. L. Wang, 2008:
627 Regional climate models downscaling analysis of general circulation models
628 present climate biases propagation into future change projections. *Geophys. Res.*
629 *Lett.*, **35**, doi:10.1029/2007GL032849.

630 Maurer, E. P., 2007: Uncertainty in hydrologic impacts of climate change in the
631 Sierra Nevada, California, under two emissions scenarios. *Clim Change*, **82**, 309-
632 325.

633 Maurer, E. P., and H. G. Hidalgo, 2008: Utility of daily vs. monthly large-scale
634 climate data: an intercomparison of two statistical downscaling methods. *Hydrol.*
635 *Earth Syst. Sci*., **12**, 551-563.

636 Maurer, E. P., and H. G. Hidalgo, 2010: The utility of daily large-scale climate
637 data in the assessment of climate change impacts on daily streamflow in
638 California. *Hydrol. Earth Syst. Sci.*, **14**, 1125-38, doi:10.5194/hess-14-1125-2010.

639 Meehl, G. A., J. M. Arblaster, and C. Tebaldi, 2005: Understanding future
640 patterns of increased precipitation intensity in climate models. *Geophys. Res.*
641 *Lett.*, **32**, L18719, doi:10.1029/2005GL023680.

642 Miller, N. L., J. Jin, N. J. Schlegel, M. A. Snyder, et al., 2009: An analysis of
643 simulated California climate using multiple dynamical and statistical techniques.
644 California Energy Commission report CEC-500-2009-017-F, August, 2009. 47 pp.

645 Muller, C. J., P. A. O'Gorman, and L. E. Back, 2011: Intensification of
646 precipitation extremes with warming in a cloud-resolving model. *J. Clim.*, **24**,
647 2784-2800.

648 Nakicenovic, N., J. Alcamo, G. Davis, B. de Vries, J. Fenhann, et al., 2000:
649 Emissions Scenarios: A special report of Working Group III of the
650 Intergovernmental Panel on Climate Change. Cambridge University Press,
651 Cambridge, UK.

652 Neiman, P. J., L. J. Schick, F. M. Ralph, M. Hughes, and G. A. Wick, 2011:
653 Flooding in western Washington: The connection to atmospheric rivers, *J.*
654 *Hydromet*., **12**, 1337–1358, doi:10.1175/2011JHM1358.1.

655 O'Gorman, P. A., and T. Schneider, 2009: The physical basis for increases in
656 precipitation extremes in simulations of 21st-century climate change. *Proc. Nat.*
657 *Acad. Sci.*, **106**, 14773-77.

658 Pal, J. S., F. Giorgi, X. Q. Bi, N. Elguindi, et al., 2007: Regional climate modeling
659 for the developing world - The ICTP RegCM3 and RegCNET. *Bull. Amer.*
660 *Meterol. Soc*., **88**, 1395.

661 Panofsky, H. A., and G. W. Brier, 1968: Some Applications of Statistics to
662 Meteorology, The Pennsylvania State University, University Park, PA, USA, 224
663 pp.

664 Pierce, D. W., T. Das, D. R. Cayan, E. P. Maurer, N. L. Miller, et al., 2012:
665 Probabilistic estimates of future changes in California temperature and
666 precipitation using statistical and dynamical downscaling. *Clim. Dyn.*, published
667 online 30 March 2012. doi 10.1007/s00382-012-1337-9.

668 Ralph, F. M., and M. D. Dettinger, 2011: Storms, floods and the science of
669 atmospheric rivers. *EOS Trans. Amer. Geophys. Union*, **92**, 265-66.

670 Ralph, F. M., and M. D. Dettinger, 2012: Historical and national perspectives on
671 extreme west coast precipitation associated with atmospheric rivers during
672 December 2010. *Bull. Amer. Meteorol. Soc.*, **93**, 783-790.

673 Salathe, E. P. Jr., 2006: Influences of a shift in North Pacific storm tracks on
674 western North American precipitation under global warming. *Geophys. Res. Lett.*,
675 **33**, L19820, doi:10.1029/2006GL026882.

676 Skamarock, W. C., J. B. Klemp, J. Duidhia, D. O. Gill, D. M. Barker, et al., 2008:
677 A description of the Advanced Research WRF Version 3. NCAR technical note
678 NCAR/TN-475+STR. 125 pp.

679 Stephens, G. L., and Y. Hu, 2010: Are climate-related changes to the character of
680 global-mean precipitation predictable? *Environ. Res. Lett.*, **5**, 025209, 7 pp.

681 Sun, Y., S. Solomon, A. Dai, and R. W. Portmann, 2006: How often does it rain?
682 *J. Clim.*, **19**, 916-934.

683 Ulbrich, U., J. G. Pinto, H. Kupfer, G. C. Leckebusch, T. Spangehl, and M.
684 Reyers, 2008: Changing Northern Hemisphere storm tracks in an ensemble of
685 IPCC climate change simulations. *J. Clim*., **21**, 1669.

686 Viale, M., and M. N. Nuñez, 2011: Climatology of Winter Orographic
687 Precipitation over the Subtropical Central Andes and Associated Synoptic and
688 Regional Characteristics. *J. Hydromet.*, **12**, 481–507.

689 Wehner, M. F., R. L. Smith, G. Bala, and P. Duffy, 2010: The effect of horizontal
690 resolution on simulation of very extreme U.S. precipitation events in a global
691 atmosphere model. *Clim. Dyn.*, **34**, 241-247.

692 Wood, A. W., E. P. Maurer, A. Kumar, and D. P. Lettenmaier, 2002: Long-range
693 experimental hydrologic forecasting for the eastern United States. *J. Geophys.*
694 *Res. Atmos.*, **107**, doi:10.1029/2001jd000659.

695 Wood, A.W., L. R. Leung, V. Sridhar, and D. P. Lettenmaier, 2004: Hydrologic
696 implications of dynamical and statistical approaches to downscaling climate
697 model outputs. *Clim Change*, **62**, 189-216.

698 Yin, J., 2005: A consistent poleward shift of the storm tracks in simulations of the
699 21st century climate. *Geophys. Res. Lett*. **32**, L18701.

700 Zhu, Y., and R. E. Newell, 1998: A proposed algorithm for moisture fluxes from
701 atmospheric rivers. *Mon. Weather Rev*., **126**, 725–735.

Table legends

Table 1. The global general circulation models (GCMs) used in this project, their originating institution, and whether they were downscaled by the indicated method. BCSD: bias correction with spatial disaggregation; BCCA: bias correction with constructed analogues; WRF: weather research forecast model; RSM: regional spectral model; RegCM3: Regional climate model version 3.

Figure legends

Figure 1. Climatological number of zero-precipitation days per year from: a) All model runs over the historical period; b) Observations, 1970-99; c) Only the dynamically downscaled runs over the historical period, with bias correction; d) Only the dynamically downscaled runs, without bias correction. Color scale is along the bottom. Panel e: histogram showing the frequency of occurrence (expressed as the percent of gridcells) experiencing the indicated number of zero-precipitation days per year.

Figure 2. Panel a: Change (future era minus historical) in annual precipitation (percent). b) Empirical cumulative distribution function (CDF) of the precipitation changes; 73% of the gridcells experience decreasing precipitation. c) Change in number of zero precipitation days per year. d) CDF of changes in number of zero-precipitation days per year; the median value is about 8 days/year. e) As panel c, but in percent. f) As panel d, but in percent. All values are averaged across all downscaling methods and models.

Figure 3. Change in the number of zero-precipitation days (days/year), future era minus historical, as a function of global model (labels on the left) and downscaling technique.

Figure 4. Colored maps: the mean ratio of downscaled to global model daily precipitation, computed on days with precipitation (the “amplification factor”). Rows correspond to the downscaling method; WRF, RSM, and RegCM3 are dynamical methods, while BCCA is a statistical method. When the downscaling method was applied to more than one global model, the mean across global

732 models is shown. Columns correspond to terciles of the global precipitation
733 amount in each gridcell for the day being downscaled. The color scale for the
734 maps is along the right hand side. Line plots: histograms of the amplification
735 factor for the different downscaling methods taken across all gridcells, for the
736 indicated tercile of global precipitation amount.

737 Figure 5. Change (future minus historical era) in the incidence of the indicated
738 precipitation rate, averaged across all model projections. Values are expressed as a
739 function of the percent of precipitating days. I.e., a value of 100% indicates that
740 twice as many precipitating days have the indicted rate.

741 Figure 6. Left panels: change (days/year) in incidence of indicated precipitation
742 intensity, future minus historical era. Right panel: the regional average of the data
743 in the left panels, as a function of precipitation intensity. The dividing latitude
744 between Northern and Southern California is taken as 36°N.

745 Figure 7. The effect of different downscaling techniques on changes (number of
746 days/year) in precipitation intensity in the lowest and highest bins from Figure 6
747 (0.1 to 5 mm/day, and 60+ mm/day, respectively). The upper set of panels shows
748 results from the GFDL CM2.1 global model; the lower set shows results from the
749 CCSM3 global model. The mean change (future – historical era) in California
750 annual precipitation obtained by each downscaling method is noted in the title.

751 Figure 8. Change in California's annual mean precipitation (mm) due to the
752 change in the number of zero precipitation days (left) and precipitation intensity
753 (middle). Right: the total annual mean change, which is equal to the sum of the
754 components shown in panels a and b. Model projection number is along the x axis.

Results using BCCA, BCSD, and dynamical downscaling are crosshatched, solid, and stippled, respectively.

Figure 9. Change in California's annual precipitation across model projections (x axis) when only days with less than the indicated precipitation rate (mm/day) are included. The percentage in the title shows the fraction of gridcell-days included for indicated cutoff. Results using BCCA, BCSD, and dynamical downscaling are crosshatched, solid, and stippled, respectively.

Figure 10. Mean model occurrence rate (expressed as 1-in-N days) of precipitation events with > 60 mm/day. a) When considering all days. b) When considering only days with precipitation. Grey areas experienced no 60 mm/day events. c) Empirical cumulative distribution function (CDF) of the values of N across all gridpoints that experienced an event with > 60 mm/day precipitation.

Figure 11. Changes in precipitation intensity vs. frequency over the annual cycle in 4 regions. Top row: Annual cycle of monthly precipitation (mm/day), for the historical (blue) and future (red) eras. The change in yearly precipitation (%) is in the title. At each month, a box is drawn between the historical and future values; the box is shaded green if the future value is wetter, and brown if it is drier. The box has a heavy outline if the difference is statistically significant at the 95% level, a normal outline if significant at the 90% level, and a light grey outline if not statistically significant. Black dots show individual model values. Middle row: Change in number of days with non-zero precipitation ("rainy days"); yellow boxes show a decrease in rainy days, while grey boxes show an increase. Bottom row: The 50th (solid line) and 95th (dashed line) percentiles of precipitation, calculated only on days when precipitation occurred, for the historical (blue) and

779 future (red) eras. The Y axis uses a square root transformation to cover the wide
780 range of values. Data from the dynamical and BCCA downscaling methods was
781 used to make the figure.

782 Figure 12. California climate regions identified by Abatzoglou et al. (2009). The
783 sub-panels in Figure 13 are plotted in accordance with the locations shown here.

784 Figure 13. Apportioning the seasonal precipitation change in each region to
785 changes in storm frequency and intensity. In each set of three bars, the left most
786 (marked "P") shows the change in precipitation during that season (cm). (For
787 comparison, the change in seasonal precipitation is shown at the bottom of each
788 subpanel, in percent.) This bar is colored green for positive (wetter future)
789 changes, and brown for negative (drier future) changes. The middle bar (“Z")
790 shows the change in seasonal precipitation (cm) that arises due to the change in
791 number of zero-precipitation days. Yellow indicates an increase in zero-
792 precipitation days, and grey indicates a decrease. The rightmost bar (marked "I")
793 shows the change in seasonal precipitation (cm) that arises from the change in
794 precipitation intensity. Red shows an increasing intensity, blue shows decreasing
795 intensity. Note that the Y axis varies by region, but for each region is the same
796 across all seasons. Sub-panel locations are illustrated in Figure 12.

Table 1

GCM	Institution	BCSD	BCCA	WRF	RSM	RegCM3
BCCR BCM 2.0	Bjerknes Centre Clim. Res., Bergen, Norway	Y				
CCCMA CGCM3.1	Canadian Centre, Victoria, B.C., Canada	Y				
CNRM CM3	Meteo-France, Toulouse, France	Y	Y			
CSIRO MK3.0	CSIRO Atmos. Res., Melbourne, Australia	Y				
GFDL CM2.0	Geophys. Fluid Dyn. Lab, Princeton, NJ, USA	Y				
GFDL CM2.1	Geophys. Fluid Dyn. Lab, Princeton, NJ, USA	Y	Y	Y	Y	Y
GISS e_r	NASA/Goddard Inst. Space Studies, N.Y., USA	Y				
INMCM 3.0	Inst. Num. Mathematics, Moscow, Russia	Y				
IPSL CM4	Inst. Pierre Simon Laplace, Paris, France	Y				
MIROC 3.2 medres	Center Climate Sys. Res., Tokyo, Japan	Y				
MIUB ECHO-G	Meteor. Inst. U. Bonn, Bonn, Germany	Y				
MPI-ECHAM5	Max Planck Inst. Meteor., Hamburg, Germany	Y				
MRI CGCM2.3.2	Meteor. Res. Inst., Tsukuba, Ibaraki, Japan	Y				
NCAR CCSM3	Nat. Center Atmos. Res., Boulder, CO, USA	Y	Y	Y	Y	
NCAR PCM1	Nat. Center Atmos. Res., Boulder, CO, USA	Y	Y			
UKMO HadCM3	UK Met Office, Exeter, Devon, UK	Y				

Table 1. The global general circulation models (GCMs) used in this project, their originating institution, and whether they were downscaled by the indicated method. BCSD: bias correction with spatial disaggregation; BCCA: bias correction with constructed analogues; WRF: weather research forecast model; RSM: regional spectral model; RegCM3: Regional climate model version 3.

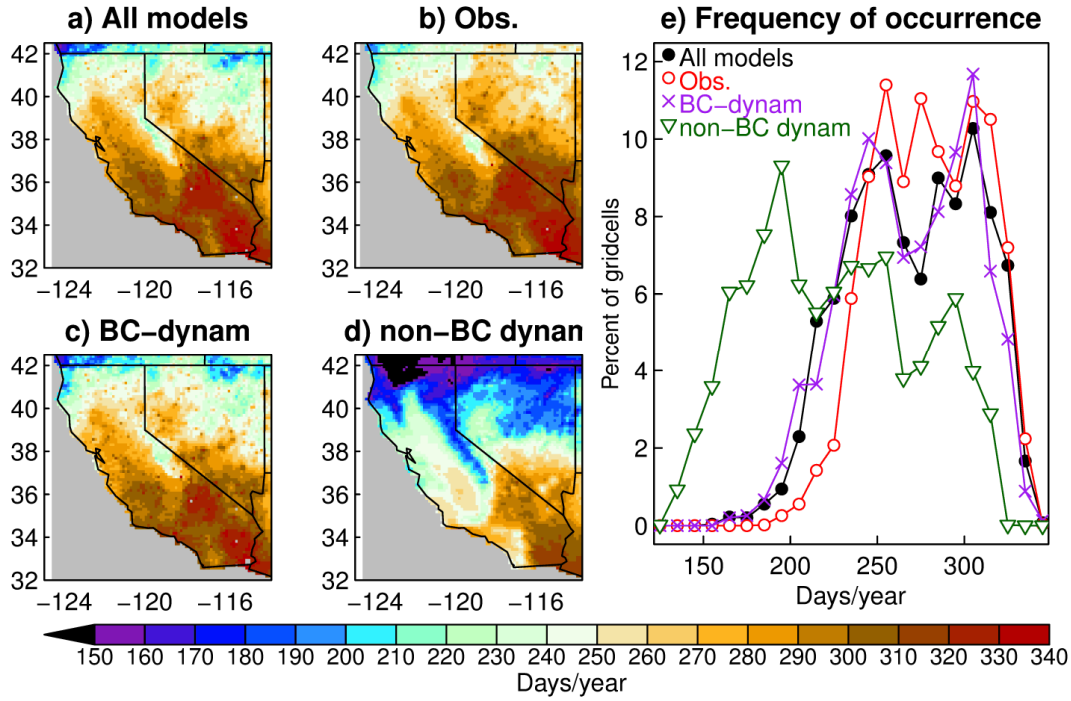

804

805 Figure 1. Climatological number of zero-precipitation days per year from: a) All
806 model runs over the historical period; b) Observations, 1970-99; c) Only the
807 dynamically downscaled runs over the historical period, with bias correction; d)
808 Only the dynamically downscaled runs, without bias correction. Color scale is
809 along the bottom. Panel e: histogram showing the frequency of occurrence
810 (expressed as the percent of gridcells) experiencing the indicated number of zero-
811 precipitation days per year.

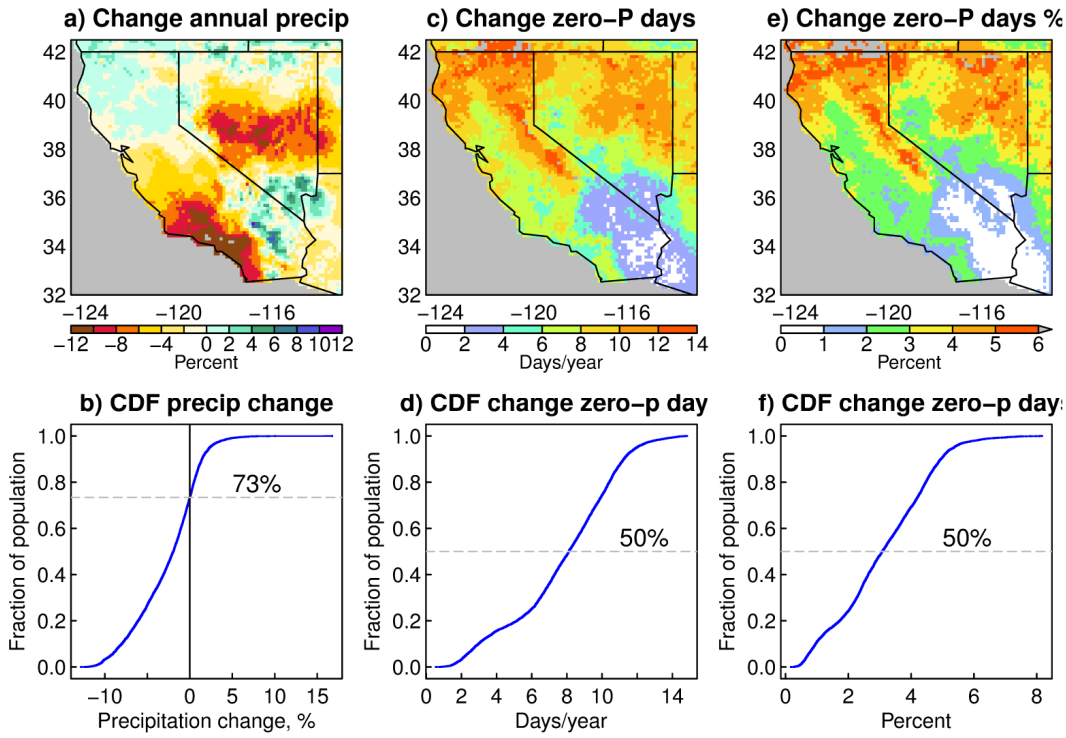

/net/puddle/data/cec_scenarios/vic_sims_dynam_corr/common_grid/rate_zero_and_mean_v7.R Wed Jan 30 14:01:36 2013

Figure 2. Panel a: Change (future era minus historical) in annual precipitation (percent). b) Empirical cumulative distribution function (CDF) of the precipitation changes; 73% of the gridcells experience decreasing precipitation. c) Change in number of zero precipitation days per year. d) CDF of changes in number of zero-precipitation days per year; the median value is about 8 days/year. e) As panel c, but in percent. f) As panel d, but in percent. All values are averaged across all downscaling methods and models.

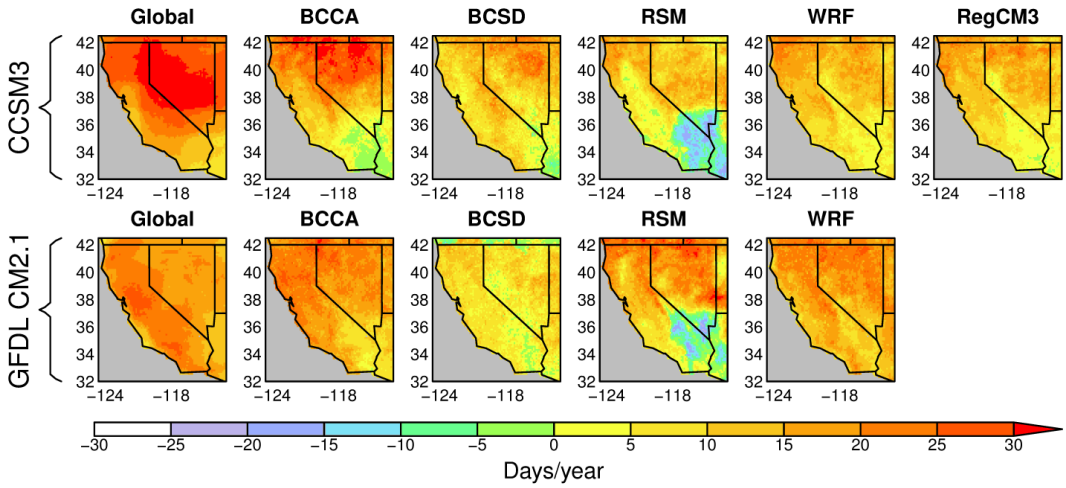

Figure 3. Change in the number of zero-precipitation days (days/year), future era minus historical, as a function of global model (labels on the left) and downscaling technique.

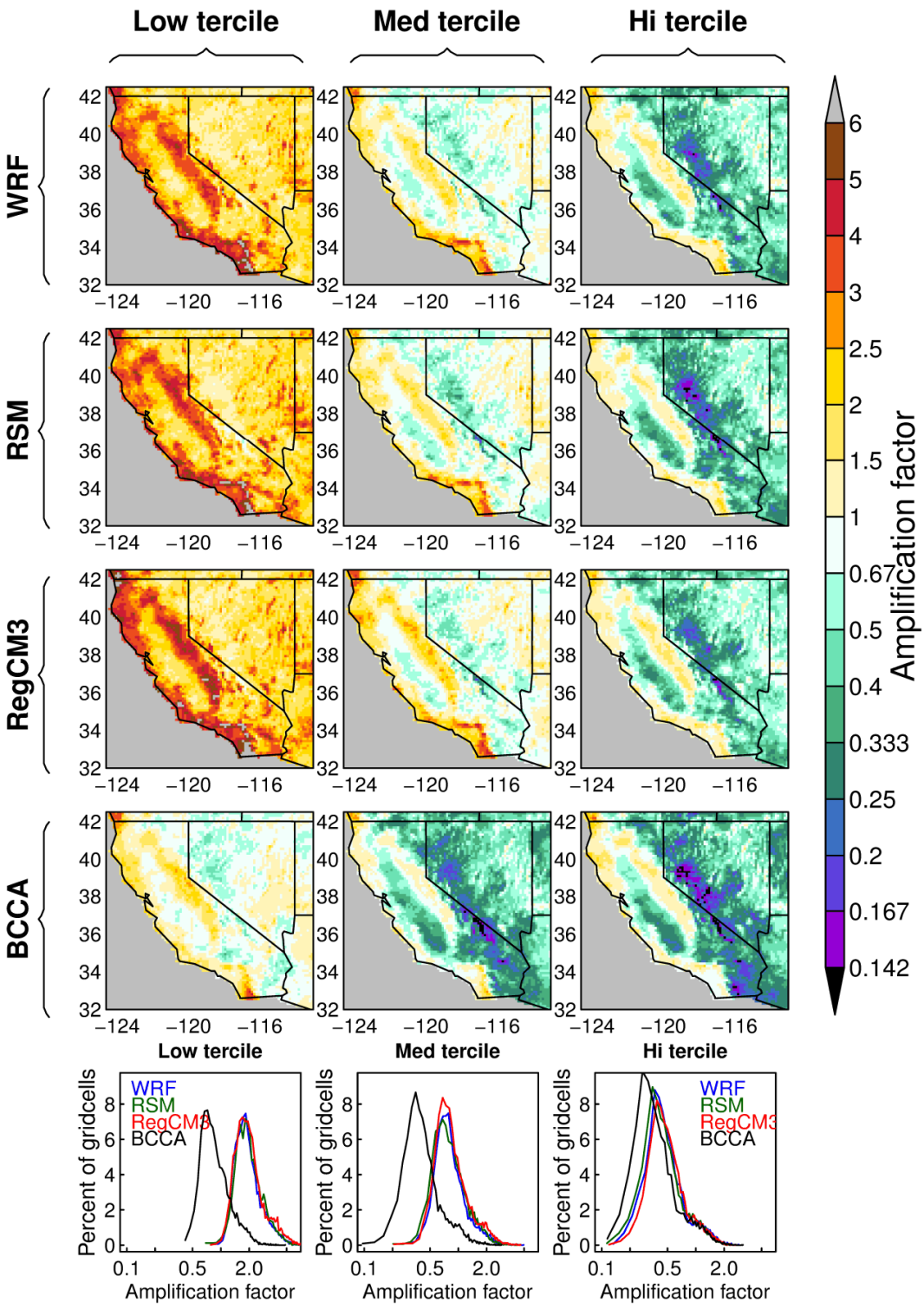

824

825 Figure 4. Colored maps: the mean ratio of downscaled to global model daily

826 precipitation, computed on days with precipitation (the "amplification factor").

827 Rows correspond to the downscaling method; WRF, RSM, and RegCM3 are

828 dynamical methods, while BCCA is a statistical method. When the downscaling

method was applied to more than one global model, the mean across global models is shown. Columns correspond to terciles of the global precipitation amount in each gridcell for the day being downscaled. The color scale for the maps is along the right hand side. Line plots: histograms of the amplification factor for the different downscaling methods taken across all gridcells, for the indicated tercile of global precipitation amount.

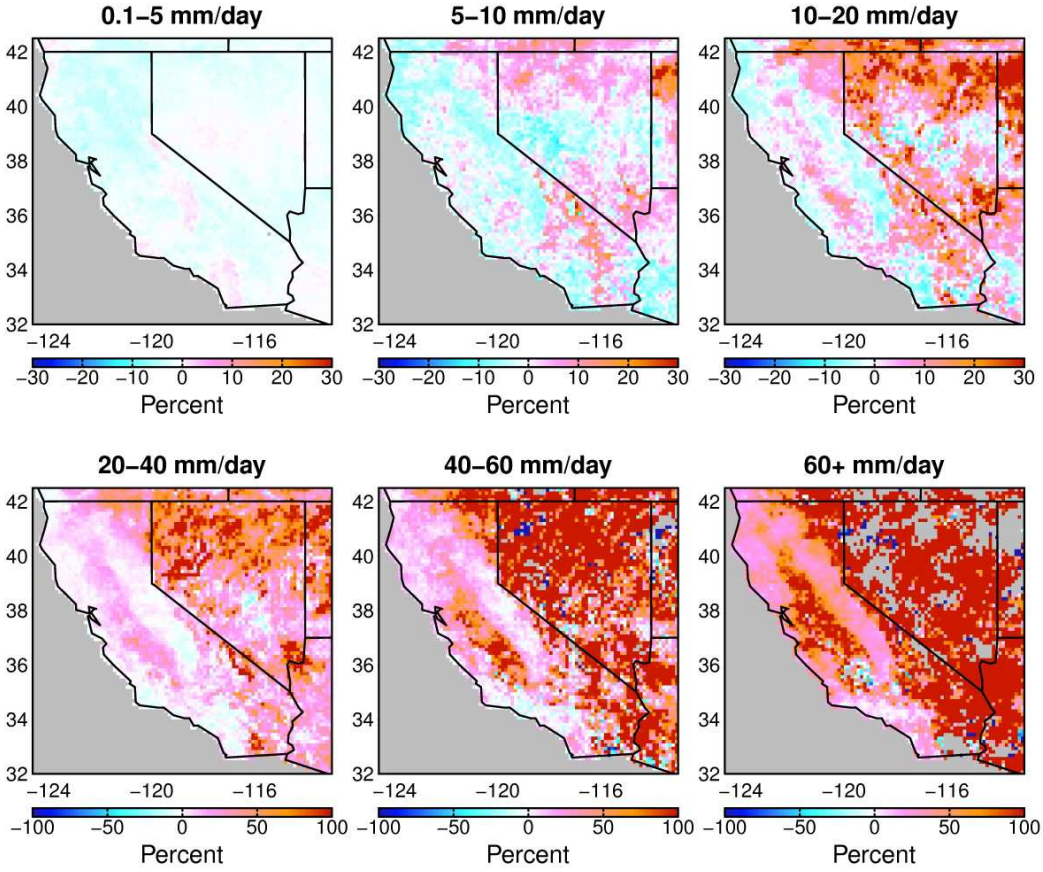

Figure 5. Change (future minus historical era) in the incidence of the indicated precipitation rate, averaged across all model projections. Values are expressed as a function of the percent of precipitating days. I.e., a value of 100% indicates that twice as many precipitating days have the indicted rate.

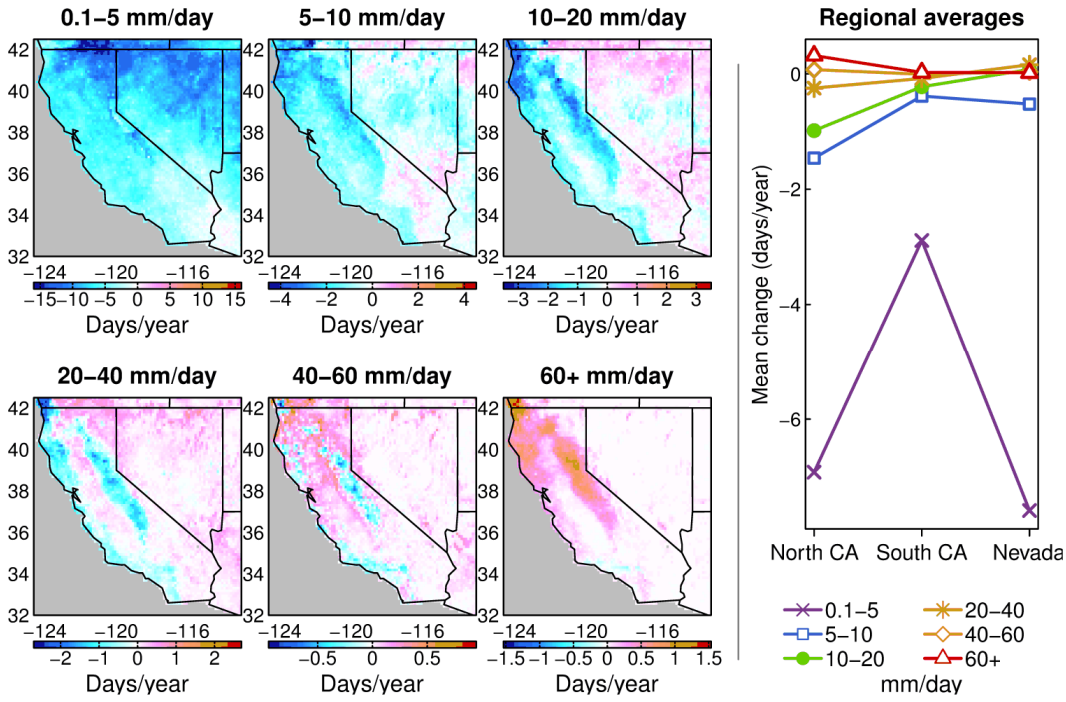

Figure 6. Left panels: change (days/year) in incidence of indicated precipitation intensity, future minus historical era. Right panel: the regional average of the data in the left panels, as a function of precipitation intensity. The dividing latitude between Northern and Southern California is taken as 36°N.

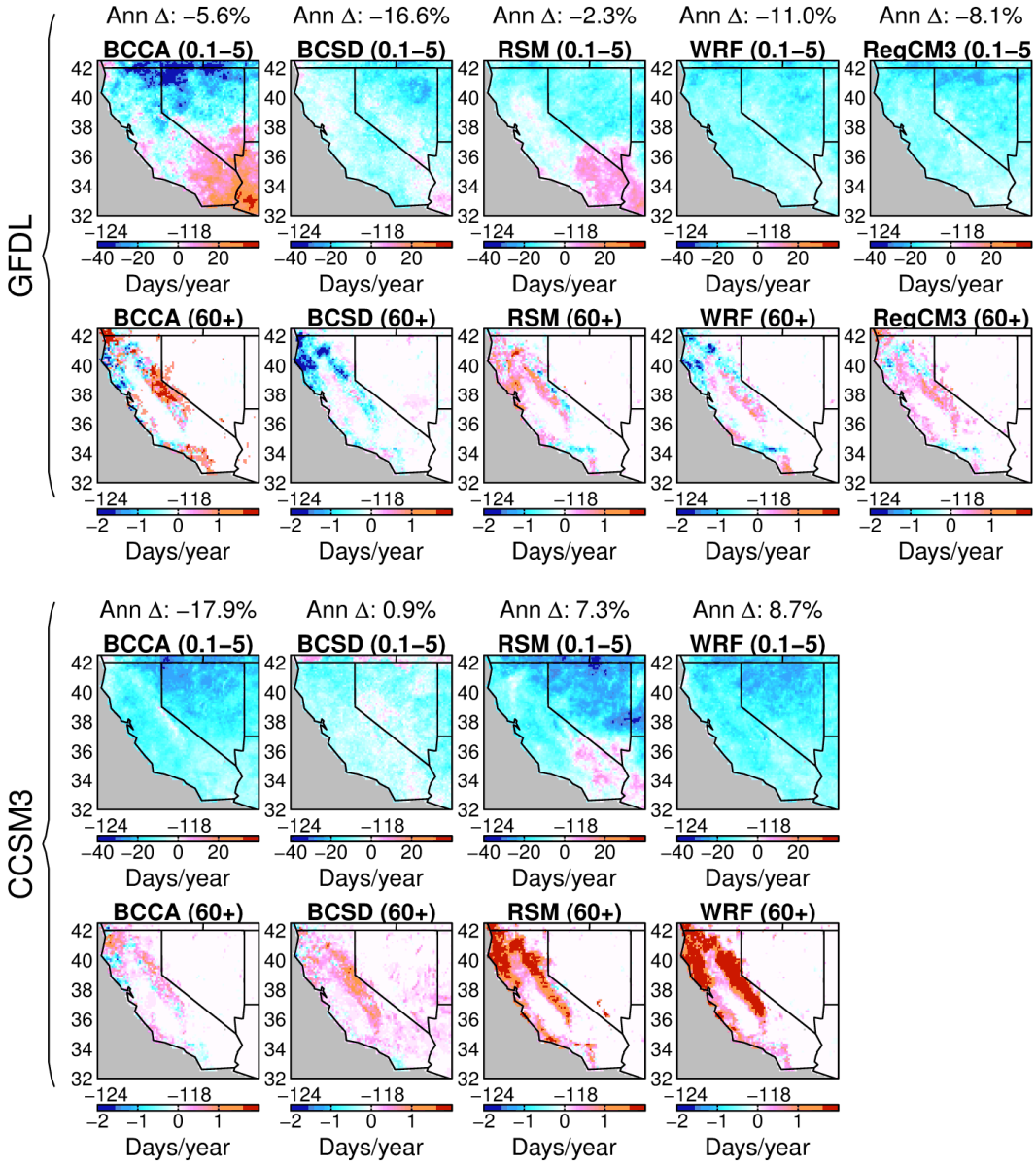

Figure 7. The effect of different downscaling techniques on changes (number of days/year) in precipitation intensity in the lowest and highest bins from Figure 6 (0.1 to 5 mm/day, and 60+ mm/day, respectively). The upper set of panels shows results from the GFDL CM2.1 global model; the lower set shows results from the CCSM3 global model. The mean change (future – historical era) in California annual precipitation obtained by each downscaling method is noted in the title.

852

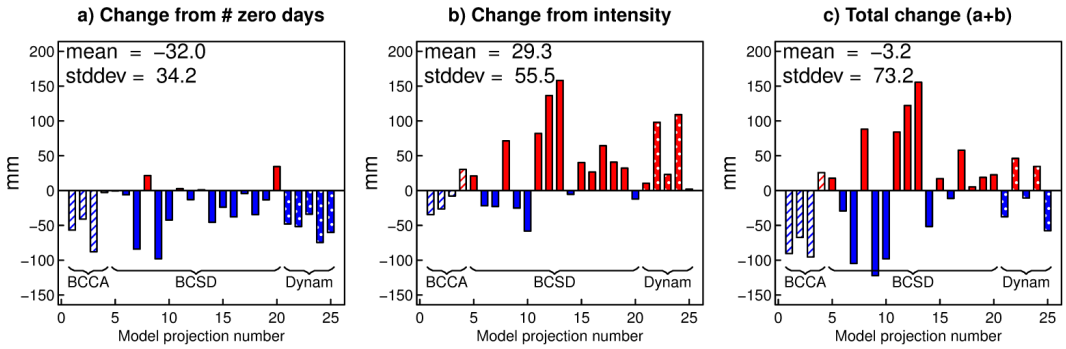

853

854 Figure 8. Change in California's annual mean precipitation (mm) due to the
855 change in the number of zero precipitation days (left) and precipitation intensity
856 (middle). Right: the total annual mean change, which is equal to the sum of the
857 components shown in panels a and b. Model projection number is along the x axis.
858 Results using BCCA, BCSD, and dynamical downscaling are crosshatched, solid,
859 and stippled, respectively.

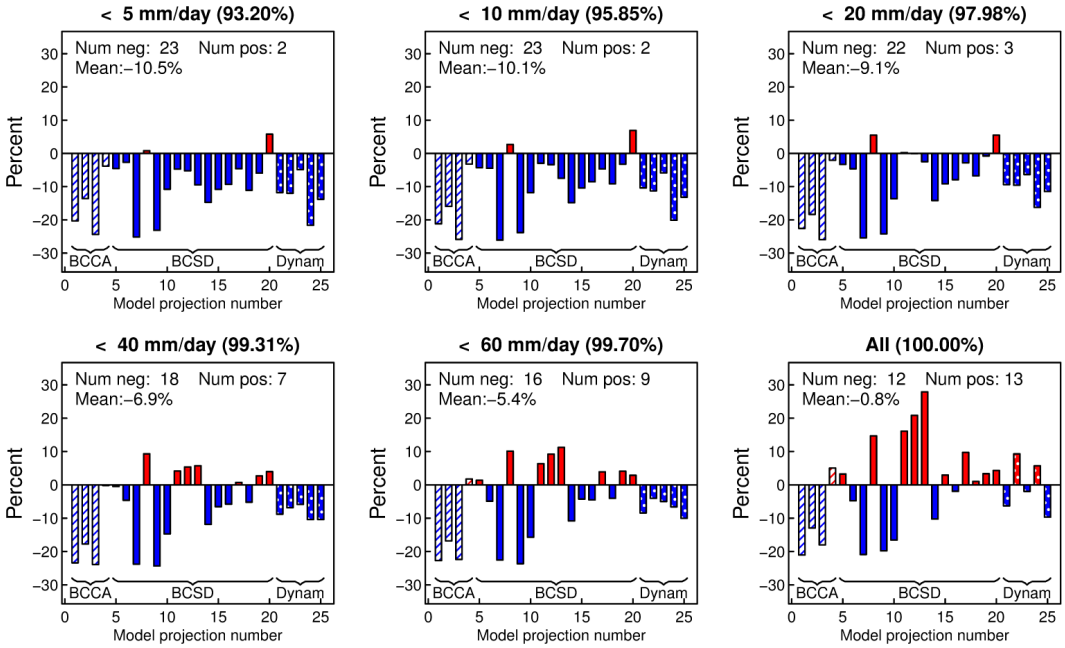

Figure 9. Change in California's annual precipitation across model projections (x axis) when only days with less than the indicated precipitation rate (mm/day) are included. The percentage in the title shows the fraction of gridcell-days included for indicated cutoff. Results using BCCA, BCSD, and dynamical downscaling are crosshatched, solid, and stippled, respectively.

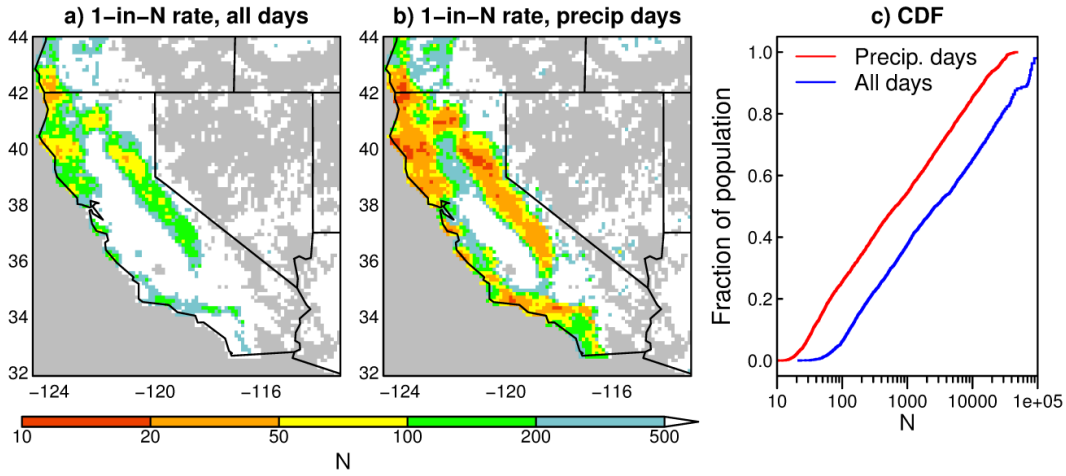

866

867 Figure 10. Mean model occurrence rate (expressed as 1-in-N days) of precipitation
868 events with > 60 mm/day. a) When considering all days. b) When considering
869 only days with precipitation. Grey areas experienced no 60 mm/day events. c)
870 Empirical cumulative distribution function (CDF) of the values of N across all
871 gridpoints that experienced an event with > 60 mm/day precipitation.

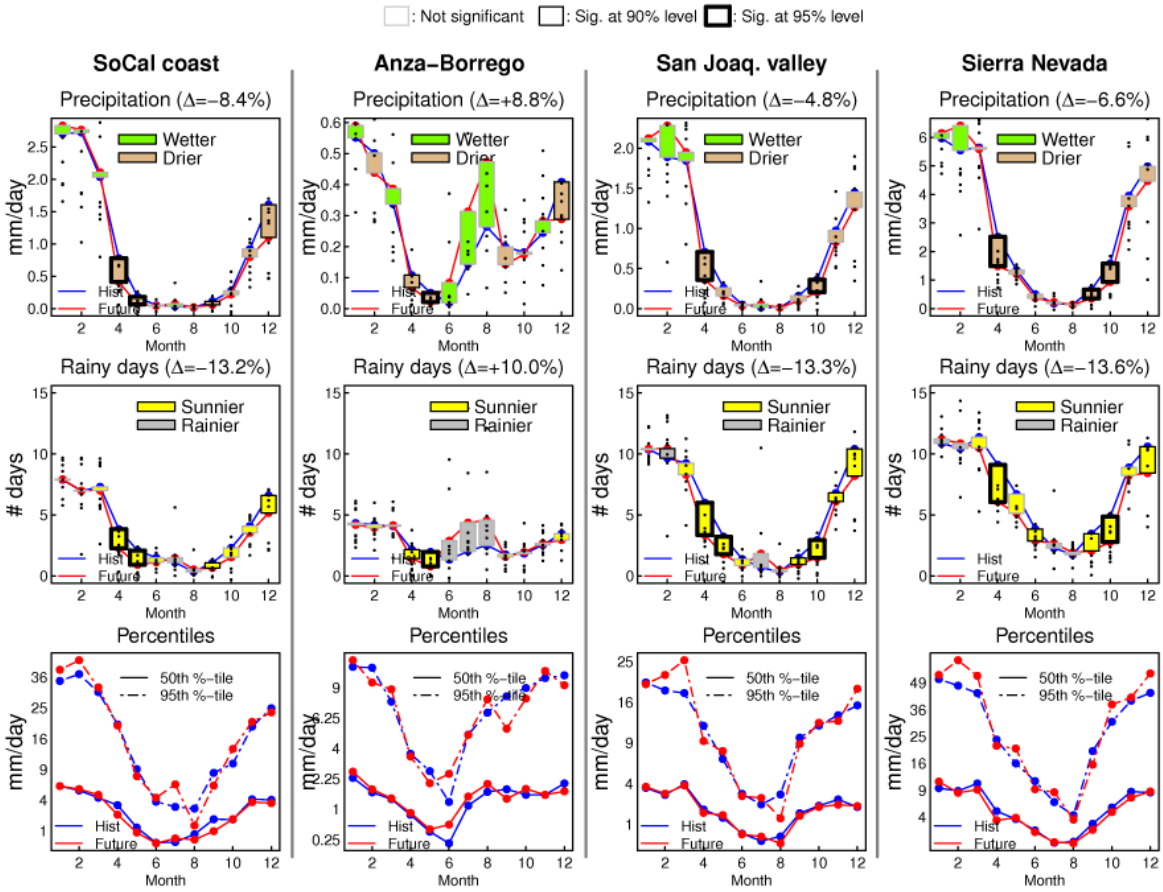

Figure 11. Changes in precipitation intensity vs. frequency over the annual cycle in 4 regions. Top row: Annual cycle of monthly precipitation (mm/day), for the historical (blue) and future (red) eras. The change in yearly precipitation (%) is in the title. At each month, a box is drawn between the historical and future values; the box is shaded green if the future value is wetter, and brown if it is drier. The box has a heavy outline if the difference is statistically significant at the 95% level, a normal outline if significant at the 90% level, and a light grey outline if not statistically significant. Black dots show individual model values. Middle row: Change in number of days with non-zero precipitation ("rainy days"); yellow boxes show a decrease in rainy days, while grey boxes show an increase. Bottom row: The 50th (solid line) and 95th (dashed line) percentiles of precipitation, calculated only on days when precipitation occurred, for the historical (blue) and future (red) eras. The Y axis uses a square root transformation to cover the wide

886 range of values. Data from the dynamical and BCCA downscaling methods was
887 used to make the figure.

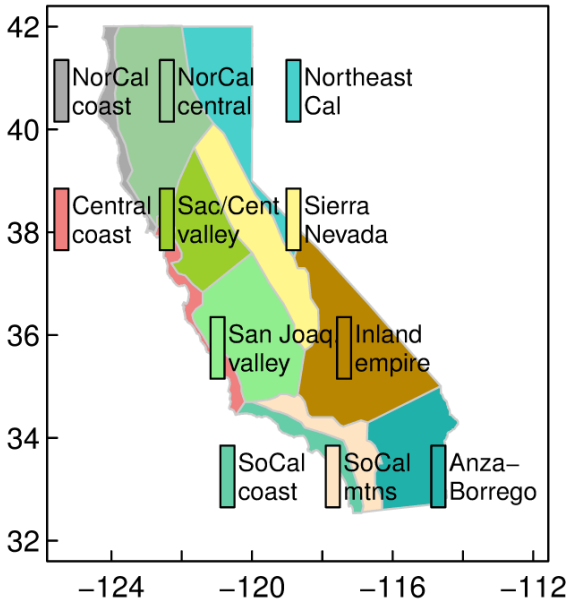

888 _climate_tracker_J_Abatzoglou/plot_regions_v4.R Tue Feb 5 10:05:58 2013

889 Figure 12. California climate regions identified by Abatzoglou et al. (2009). The

890 sub-panels in Figure 13 are plotted in accordance with the locations shown here.

Figure 13. Apportioning the seasonal precipitation change in each region to changes in storm frequency and intensity. In each set of three bars, the left most (marked "P") shows the change in precipitation during that season (cm). (For comparison, the change in seasonal precipitation is shown at the bottom of each subpanel, in percent.) This bar is colored green for positive (wetter future) changes, and brown for negative (drier future) changes. The middle bar (“Z") shows the change in seasonal precipitation (cm) that arises due to the change in number of zero-precipitation days. Yellow indicates an increase in zero-precipitation days, and grey indicates a decrease. The rightmost bar (marked "I")

shows the change in seasonal precipitation (cm) that arises from the change in precipitation intensity. Red shows an increasing intensity, blue shows decreasing intensity. Note that the Y axis varies by region, but for each region is the same across all seasons. Sub-panel locations are illustrated in Figure 12.